Supplementary Information

A supramolecular strategy to precisely fabricate binary-doping metal-free graphdiyne for high-performance zinc-air batteries

Zecheng Xiong, †[a,b] Fuhui Wang, †[a,b] Yan Zeng,[a,b] Hao Sun,[a,b] Weiyue Jin,[a,b] Hongye Liu,[a,b] Yang Huang,[a,b] Yuanping Yi,[a,b] and Huibiao Liu*[a,b]

[a] *Beijing National Laboratory for Molecular Sciences, CAS Research/Education Center for Excellence in Molecular Sciences, CAS Key Laboratory of Organic Solids, Institute of Chemistry, Chinese Academy of Sciences, Zhongguancun North First Street 2, Beijing, China*

[b] *University of Chinese Academy of Sciences, No. 19 (A) Yuquan Road, Beijing, China*

†These authors contributed equally

*E-mail: liuhb@iccas.ac.cn

Experimental

Synthesis of 1,3,5-trifluoro-2,4,6-tris[(trimethylsilyl)ethynyl] benzene

Diisopropylamine (100 mL), THF (50 mL), 1,3,5-trifluoro-2,4,6-triiodobenzene (10 mmol, 5.0977 g), $PdCl_2(PPh_3)_2$ (0.75 mmol, 530 mg), and CuI (0.75 mmol, 140 mg) were added to a dry three-necked flask, and the mixture was stirred under argon. A solution of ethynyltrimethylsilane (60 mmol, 8.4 mL) was added dropwise, followed the mixture was warmed to 60 °C and stirred for 72 h under argon. The reaction process was monitored by thin-layer chromatogram analysis (TLC). After the reaction, the reaction liquid was dried by rotary evaporator, extracted with ethyl acetate, washed with saturated salt water for three times, and dried with Na_2SO_4 (anhydrous). Then the crude product was washed with methanol to obtain light yellow powder, which was separated by column silica gel (the eluent was petroleum ether/dichloromethane, volume ratio was 20:1), to obtain white crystalline powder 1,3,5-trifluoro-2,4,6-tris[(trimethylsilyl)ethynyl] benzene.

Synthesis of 1,3,5-trifluoro-2,4,6-triethynyl-benzene

Tetrahydrofuran (30 mL) and methanol (30 mL) were added into a two-necked flask, protected by argon, 1,3,5-trifluoro-2,4,6-tris[(trimethylsilyl)ethynyl] benzene (0.24 mmol, 100 mg) was added, stirred at room temperature and dissolved for at least 30 minutes, then saturated potassium carbonate aqueous solution (3 mL) was added. After reaction in dark for 5 minutes, it was extracted with ethyl acetate immediately and washed with saturated salt water for several times, and dried with Na_2SO_4 (anhydrous). After rotary drying, the crude product was separated by column silica gel (eluent: petroleum ether), and white crystalline powder 1,3,5-trifluoro-2,4,6-triethynyl-benzene was obtained. It was prepared and used now, and stored in inert environment at low temperature

Synthesis of GDY-3F

Pyridine (100 mL) was added to the dry and clean three-necked flask, protected by argon. The cleaned copper foils were put into the reaction bottle, which were

completely immersed in the reaction solution. Slowly dropped the pyridine solution which was dissolved with 1,3,5-trifluoro-2,4,6-triethynyl-benzene, and then rose to 80 ℃, and reacted continuously for 3 days in the atmosphere of argon. The black film on the copper foil is trifluoro-graphdiyne (GDY-3F). Trifluoro-graphdiyne powder was obtained by ultrasonic stripping of trifluoro-graphdiyne from copper foil, drying reaction solution by rotary evaporation, and washing with acetone, acetonitrile and methanol for several times.

Synthesis of supramolecular systems of GDY-3F

Pyridine (100 mL) was added to the dry and clean three-necked flask, protected by argon. And excessive melamine (0.79 mmol, 100 mg) or 1,3,5-triaminobenzene ($3NH_2$-Ben, 0.81 mmol, 100 mg) was added, stirred continuously to form a homogeneous solution. The cleaned copper foils were put into the reaction bottle, which were completely immersed in the reaction solution, and stop stirring. Slowly dropped the pyridine solution which was dissolved with 1,3,5-trifluoro-2,4,6-triethynyl-benzene, then rose to 80 ℃, and reacted continuously for 3 days in the atmosphere of argon. The black film of GDY-3F-Melamine or GDY-3F-$3NH_2$-Ben was obtained on the copper foil after three days of continuous reaction in argon atmosphere and one day of stirring reaction. The product on copper foil was peeled by ultrasonic wave, dried reaction solution by rotary evaporation, and then washed with acetone, acetonitrile and methanol for several times. The product was GDY-3F-Melamine or GDY-3F-$3NH_2$-Ben powder.

Characterization

Transmission electron microscopy (TEM), high resolution transmission electron microscopy (HRTEM) images and elemental mapping results were obtained on a JEM-2100F electron microscope operating at 200 kV. Raman spectra was recorded on a NT-MDT NTEGRA Spectra system, with the excitation from an Ar laser at 473 nm. X-ray photoelectron spectroscopy (XPS) was performed using a VG Scientific ESCALab220i-XL X-ray photoelectron spectrometer, with Al Kα radiation as the excitation source. Ultraviolet-visible absorption (UV-vis) spectra were taken on a

SHIMADZU UV-2600 spectrophotometer equipped with integrating sphere attachment. The UV absorption spectrum was obtained by Kubelka-Munk formula conversion.

Electrocatalytic performance test

The ORR/OER performance of the catalysts were characterized by the rotating disk electrode device (RDE, pine instruments, Inc.) with the electrochemical workstation CHI 760D. All electrochemical measurements were performed in a conventional three-electrode system, using glassy carbon electrode loaded with catalyst as the working electrode, platinum plate (1×1 cm^2) as the counter electrode, and Ag/AgCl as the reference electrode, oxygen-saturated 0.1 M KOH as electrolyte. The potentials reported in this work were calibrated to RHE, using the following equation: $E_{RHE} = E_{Ag/AgCl} + 0.9646$ V.

The working electrode was a glassy carbon electrode (Φ = 3 mm) covered with catalyst. The preparation process of the electrode was as follows: 1 mg of as-prepared catalyst were ultrasonically dispersed in 250 μL isopropanol and 230 μL water, followed by the addition of 20 μL Nafion aqueous solution (5 wt%) into the solution. The mixture was ultrasonicated to obtain a homogeneous catalyst ink. Certain amount of the catalyst ink was then transferred onto the glassy carbon rotating disk electrode to ensure a constant catalyst mass loading of 0.2 mg cm^{-2} for all the measurements. The electrodes were then dried in air and served as a working electrode.

The ORR/OER catalytic performance of the catalysts were tested by cyclic voltammetry (CV) and linear sweep voltammetry (LSV), the scanning rate was 10 - 120 mV s^{-1}, the rotating speed of rotating disk electrode was 100 - 2500 rpm, and oxygen was continuously injected during the test.

The electron transfer number during the ORR process was calculated via Koutecky-Levich equation (1):[1]

$$\frac{1}{j} = \frac{1}{j_k} + \frac{1}{B\omega^{1/2}} \qquad (1)$$

where j is the measured current density, j_k is the kinetic current density, ω is the angular

velocity of RDE. Parameter B is determined by equation (2):

$$B = 0.62nFC_0D_0^{2/3}V^{-1/6} \quad (2)$$

where n is the electron transport number, F is the Faraday constant (F = 96485 C mol^{-1}), C_0 is the concentration of O_2 in bulk solution (C_0 = 1.2 × 10^{-6} mol cm^{-3}), D_0 is the diffusion coefficient of O_2 in 0.1 M KOH solution (D_0 = 1.9 × 10^{-5} cm^2 s^{-1}), V is the kinematic viscosity of the solution (V = 0.01 cm^2 s^{-1}).

Zinc-air battery assembly and testing

Zn-air batteries were assembled with Zn foil as the anode, catalytic coated carbon cloth/gas diffusion layer as the air electrode, and 6.0 M KOH + 0.2 M $Zn(CH_3COO)_2$ as the electrolyte. The catalytic layer was composed of catalyst, conductive carbon black and polyvinylidene fluoride (PVDF) adhesive (mass ratio is 6:3:1). The preparation method was as follows: 60 mg of catalyst (supramolecular system of graphdiyne) and 20 mg of conductive carbon black are evenly mixed by grinding, 260 mg of PVDF dissolved in N-methyl-pyrrolidone solution (mass ratio is 1:25) was added, mixed and stirred to form a uniform slurry, and then evenly coated on the current collector of carbon paper, then vacuum dried at 60 ℃. The prepared catalyst collector layer and gas diffusion layer were cut into the same size and pressed together with a roller press to form an air electrode. The catalyst loading in the air electrode was about 2 mg cm^{-2}.

The open circuit voltage and charge-discharge curve were tested by electrochemical workstation CHI 660E. The specific capacity, constant current discharge performance, rate performance and cycle performance were tested by LAND CT2001A battery test system. All zinc-air batteries were tested under ambient atmosphere at room temperature, and the circulating pump was used to update the electrolyte continuously which flow rate was 10 mL min^{-1}.

Computational methods

In this study, all the density functional theory (DFT) calculations for the crystal

structures were performed using the Vienna Ab initio Simulation Package (VASP 5.4.1). The projector augmented wave (PAW) method with the Perdew−Burke−Ernzerhof including dispersion (PBE-D3) exchange-correlation functional was used. Plane-wave cutoff energy of 600 eV and energy convergence criterion of 10^{-4} eV was adopted for the self-consistent cycle throughout calculations. For the GDY-3F unit cell, a vacuum region of 20 Å was included in the out-of-plane direction. To simulate doping, we first optimized the geometries of the isolated dopant molecule ($3NH_2$-Ben or Melamine) by using the B3LYP functional and the 6-31G** basis set with Gaussian 16 program. Then, we build a 2×2×1 supercell and adsorb one dopant molecule with the backbone parallel to the GDY-3F at the distance of 0 Å. Uniform 5×5×1 Gamma-centered Monkhorst-Pack k-point meshes were employed for all the systems.

Calculation of Gibbs free energy

To construct the free energy diagram of GDY-3F-Melamine system, the following four ORR steps in alkaline solution were proposed:[2,3]

$* + O_2\,(g) + H_2O\,(l) + e^- \rightarrow *OOH + OH^-,\ \Delta G_1$ (1)

$*OOH + e^- \rightarrow *O + OH^-,\ \Delta G_2$ (2)

$*O + H_2O\,(l) + e^- \rightarrow *OH + OH^-,\ \Delta G_3$ (3)

$*OH + e^- \rightarrow OH^- + *,\ \Delta G_4$ (4)

In these steps, the symbol "*" represented for the GDY-3F-Melamine substrate. The corresponding ORR intermediates were therefore marked as "*OOH", "*O", "*OH", respectively.

We chose 7 typical sites of GDY-3F-Melamine system for simulation (C1 to C7, Fig. S12a). The adsorption process of the intermediate OOH to each site was first calculated. Corresponding results indicated that C1 exhibited adsorption ability of OOH (Fig. S12b), while site C2 to C7 showed quite limited adsorption of OOH as the intermediate tended to be away from the substrate rather than be adsorbed, resulting in unstable adsorption models. Fig. S12c and 12d were displayed to demonstrate such unstable trend of OOH intermediate at site C2 and C3. Therefore, only the free energy diagram

of C1 was displayed in this manuscript. The atomic configurations of ORR intermediates *O and *OH at C1 were exhibited in Fig. S13.

To calculate the reaction Gibbs free energy of each step (ΔG_i, i = 1, 2, 3, 4), we first calculated the adsorption energies of each ORR intermediate based on equation (5) to (7):

$$\Delta E_{*OOH} = E(*OOH) - E(*) - [2E(H_2O, l) - \frac{3}{2}E(H_2, g)] \quad (5)$$

$$\Delta E_{*O} = E(*O) - E(*) - [E(H_2O, l) - E(H_2, g)] \quad (6)$$

$$\Delta E_{*OH} = E(*OH) - E(*) - [E(H_2O, l) - \frac{3}{2}E(H_2, g)] \quad (7)$$

Herein, $E(*)$, $E(*OOH)$, $E(*O)$ and $E(*OH)$ represented for the calculated total energies of the substrate and each ORR intermediate, respectively. H_2O (l) and H_2 (g) were used as the references to calculate the energy of each unadsorbed ORR intermediate.

Subsequently, the corresponding adsorption Gibbs free energies were calibrated by introducing the zero-point energy correction (ΔZPE) and entropy (ΔS). Moreover, an energy of -0.22 eV was adopted to correct the solvation effect for *OOH and *OH, demonstrating the hydrogen bonds these intermediates might form with water.[4,5] The adsorption Gibbs free energy of each intermediate was thus calculated based on equation (8) to (10):

$$\Delta G_{*OOH} = \Delta E_{*OOH} + \Delta ZPE_{*OOH} - T\Delta S_{*OOH} - 0.22 \text{ eV} \quad (8)$$

$$\Delta G_{*O} = \Delta E_{*O} + \Delta ZPE_{*O} - T\Delta S_{*O} \quad (9)$$

$$\Delta G_{*OH} = \Delta E_{*OH} + \Delta ZPE_{*OH} - T\Delta S_{*OH} - 0.22 \text{ eV} \quad (10)$$

For each intermediate, the corresponding ΔZPE – $T\Delta S$ were 0.40, 0.05 and 0.35 eV, respectively.[4]

Finally, the reaction Gibbs free energies of the proposed steps (ΔGi, i = 1, 2, 3, 4) in alkaline solution (pH = 14.0) at 0 V (*vs.* standard hydrogen electrode, SHE) were calculated based on equation (11) to (14):[3,4]

$$\Delta G_1 = \Delta G_{*OOH} + 2\Delta G_w + \Delta G_{pH} \quad (11)$$

$$\Delta G_2 = \Delta G_{*O} - \Delta G_{*OOH} + \Delta G_{pH} \quad (12)$$

$$\Delta G_3 = \Delta G_{*OH} - \Delta G_{*O} + \Delta G_{pH} \quad (13)$$

$\Delta G_4 = -\Delta G_{*OH} + \Delta G_{pH}$ (14)

In these equations, ΔG_w = -2.46 eV was the standard Gibbs formation energy of water; ΔG_{pH} was the Gibbs free energy originated from the entropy difference caused by the different concentration of H^+. In this case, pH = 14.0 was adopted, and the corresponding ΔG_{pH} was calculated as:

$\Delta G_{pH} = -k_B T \times \ln [H^+] = 0.828$ eV,

where $k_B = 8.6173303 \times 10^{-5}$ eV is the Boltzmann constant.

Fig. S14 shows the free energy diagram of ORR pathway of GDY-3F-Melamine at site C1 based on the calculated ΔG_is.

Supplementary figures and tables

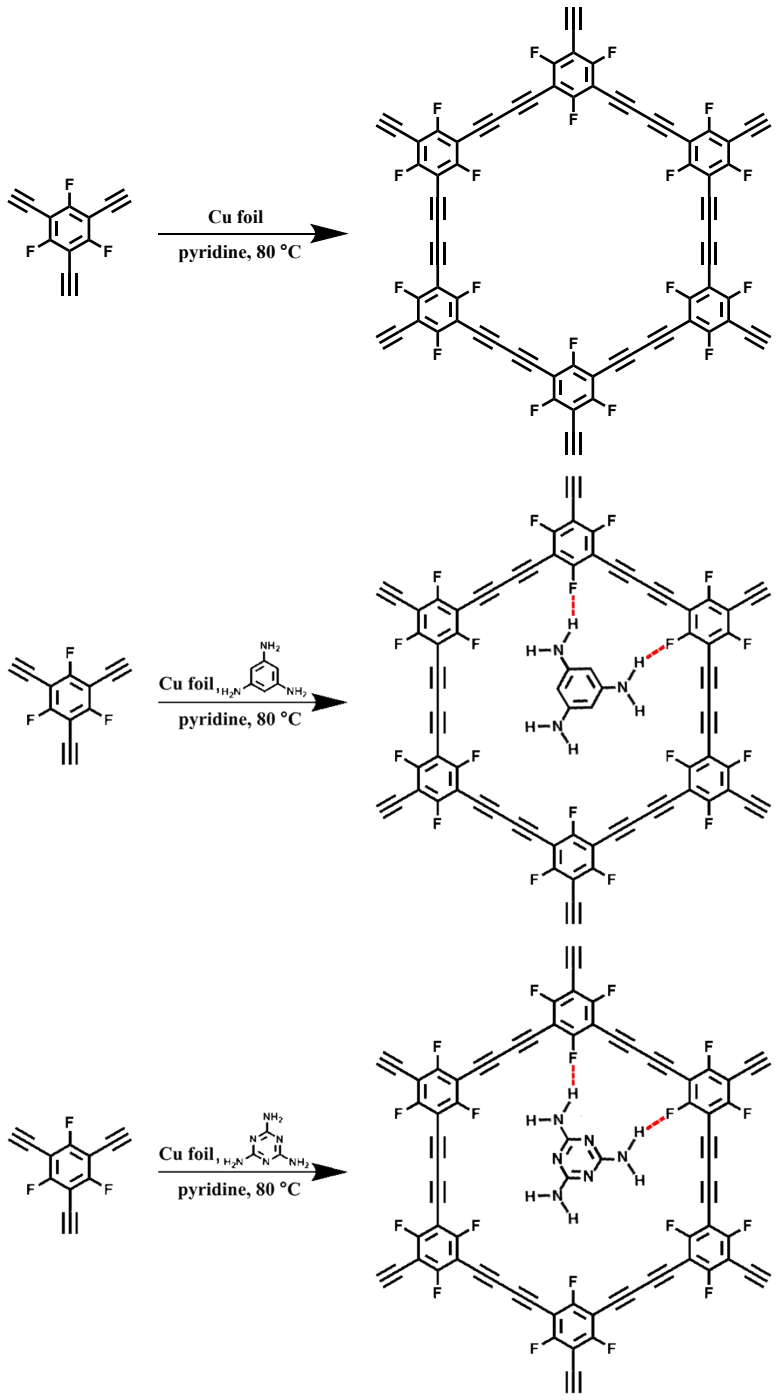

Fig. S1 Preparation of GDY-3F, GDY-3F-3NH_2-Ben, GDY-3F-Melamine.

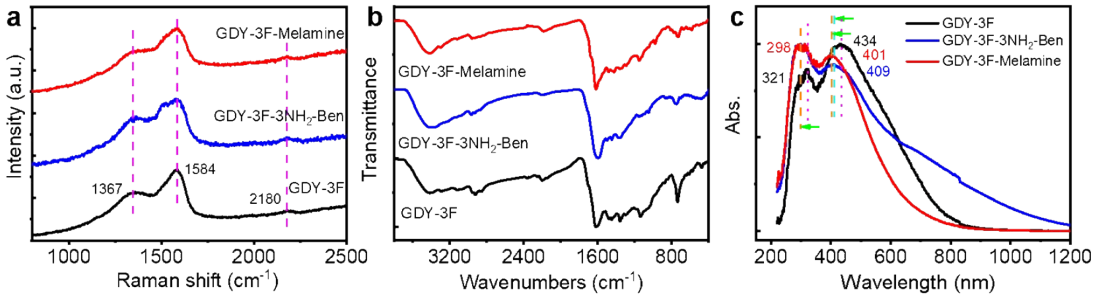

Fig. S2 Spectrogram of GDY-3F, GDY-3F-3NH_2-Ben, and GDY-3F-Melamine. (a) Raman spectroscopy, (b) FTIR spectroscopy, (c) UV-Vis absorption spectroscopy.

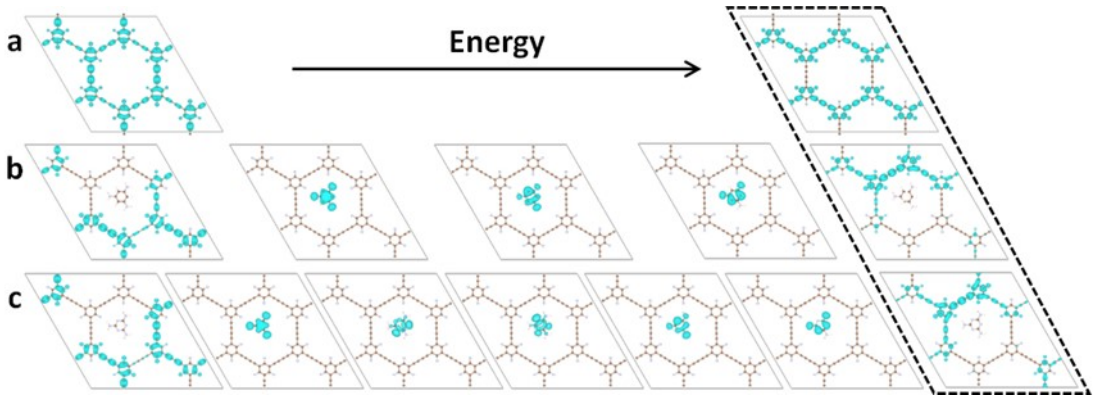

Fig. S3 Charge densities of (a) GDY-3F, (b) GDY-3F-3NH2-Ben, and (c) GDY-3F-Melamine. The charge densities at the conduction band minimum (CBM) are marked by the dashed line box.

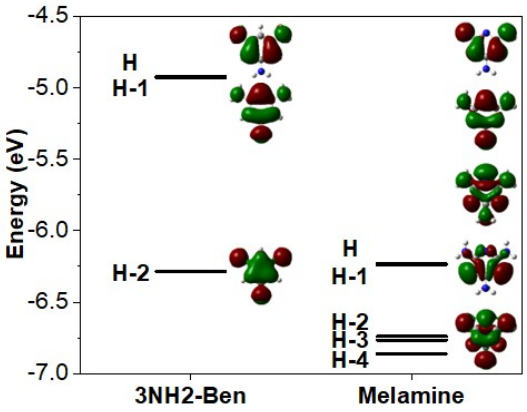

Fig. S4 Energy level diagram and pictorial representation of the highest occupied orbitals for the guest molecules.

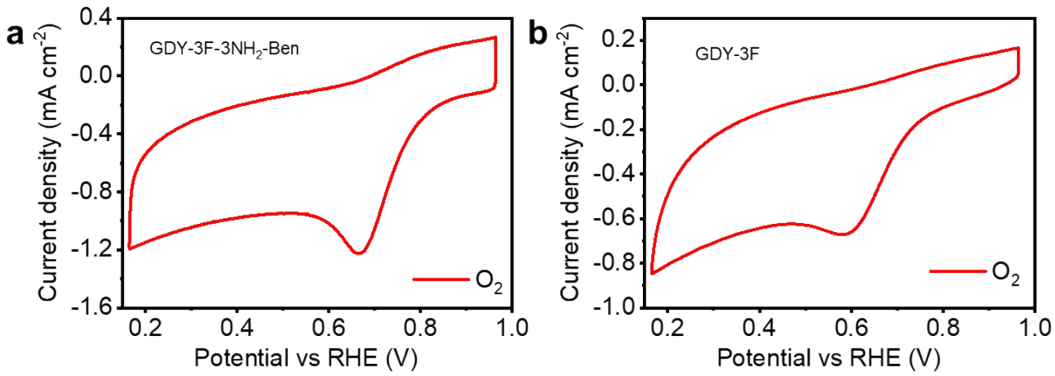

Fig. S5 Cyclic voltammetry curves. (a) GDY-3F-3NH_2-Ben, (b) GDY-3F under the condition of O_2-saturated electrolyte.

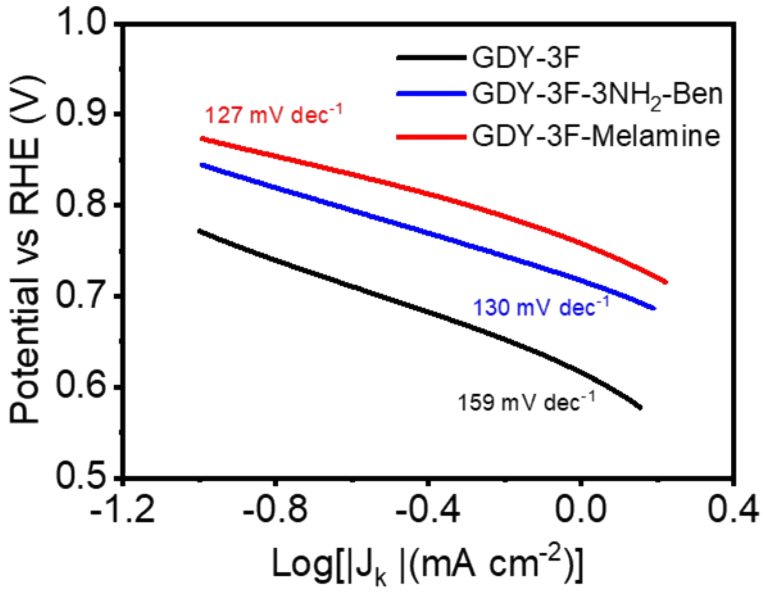

Fig. S6 Tafel plots of the supramolecular system of graphdiyne obtained from ORR electrochemical performance.

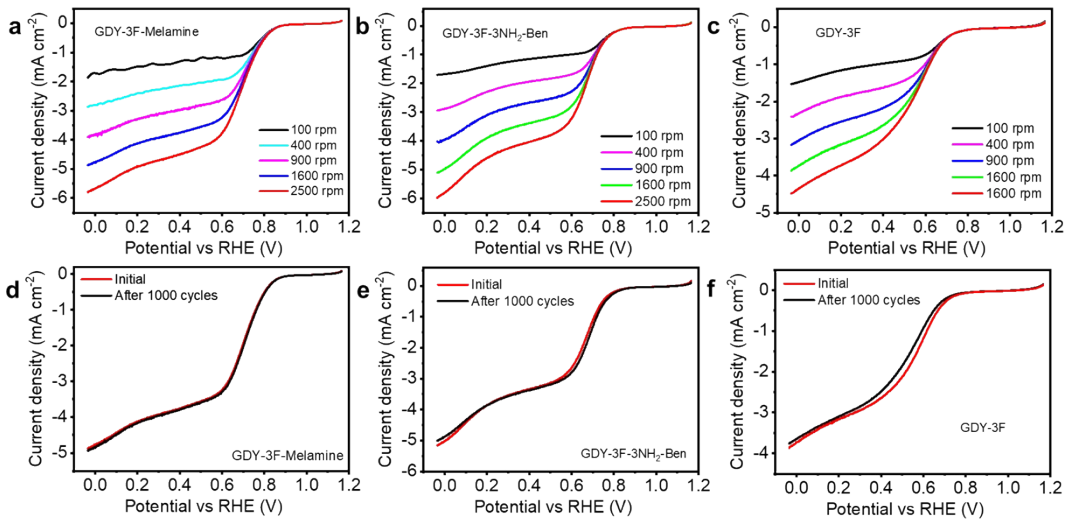

Fig. S7 LSV polarization curves. (a) GDY-3F-Melamine, (b) GDY-3F-3NH_2-Ben, (c) GDY-3F at different rotating speeds, (d)-(f) Comparison of LSV curves of different samples before and after 1000 cycles of accelerated cyclic voltammetry test.

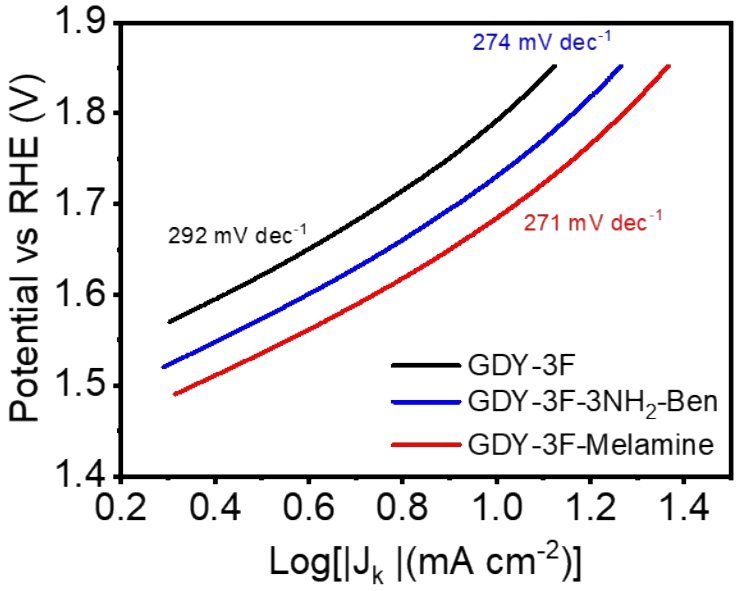

Fig. S8 Tafel plots of the supramolecular system of graphdiyne obtained from OER electrochemical performance.

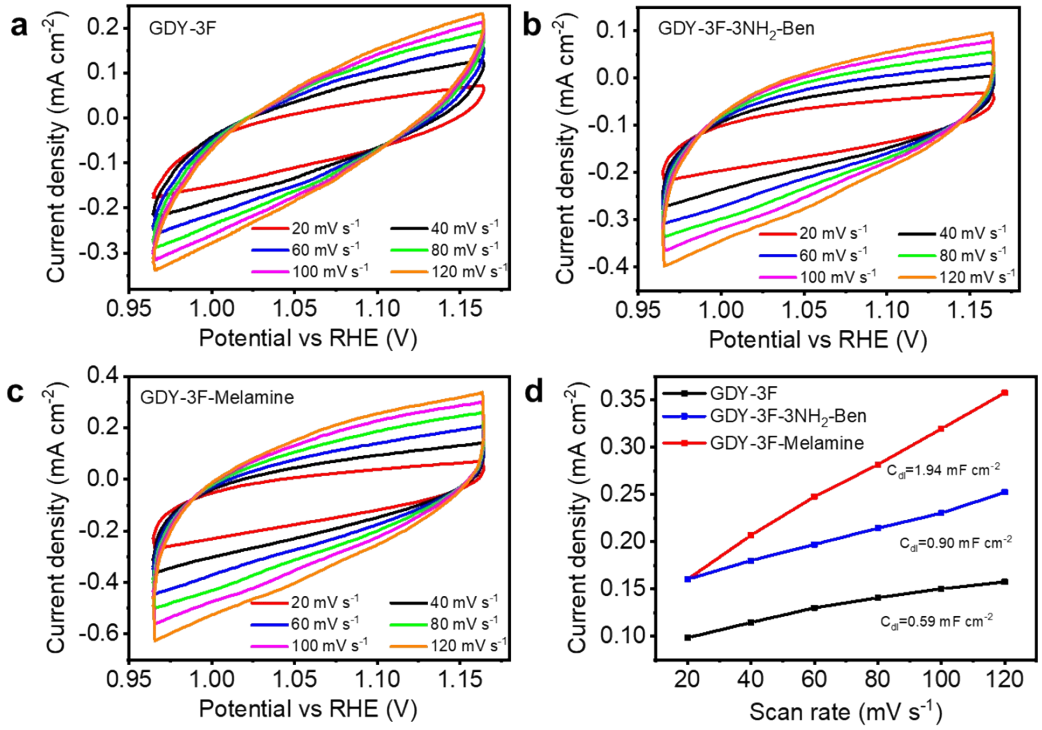

Fig. S9 Determination of double layer capacitance and electrochemical surface area (ECSA). Cyclic voltammetry curves of the as-prepared samples at the different scan rates: (a) GDY-3F, (b) GDY-3F-3NH_2-Ben, (c) GDY-3F-Melamine. (d) Corresponding capacitive current densities as a function of scan rates for supramolecular system of graphdiyne.

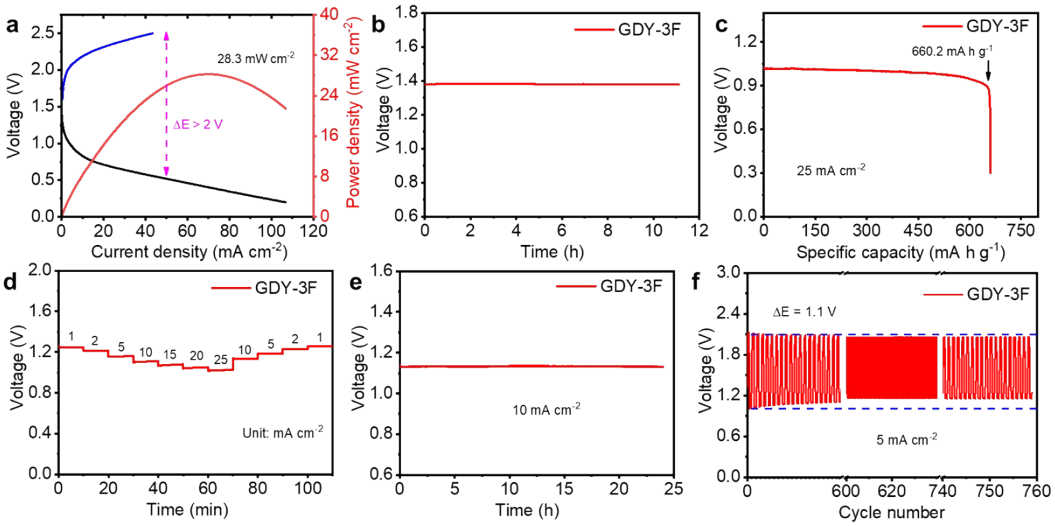

Fig. S10 Zinc-air battery performance of GDY-3F. (a) charge-discharge polarization curve and power density, (b) open-circuit voltage stability, (c) discharge curve at 25 mA cm^{-2}, (d) discharge platforms with different current densities, (e) constant discharge curve at current density of 10 mA cm^{-2}, (f) circulating charge-discharge curve at 5 mA cm^{-2}.

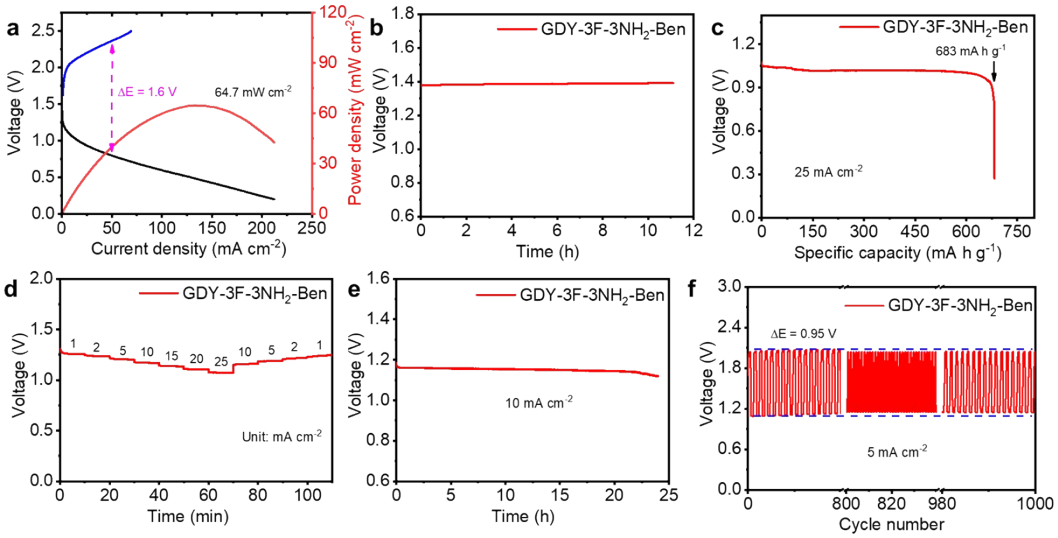

Fig. S11 Zinc-air battery performance of GDY-3F-3NH_2-Ben. (a) charge-discharge polarization curve and power density, (b) open-circuit voltage stability, (c) discharge curve at 25 mA cm^{-2}, (d) discharge platforms with different current densities, (e) constant discharge curve at current density of 10 mA cm^{-2}, (f) circulating charge-discharge curve at 5 mA cm^{-2}.

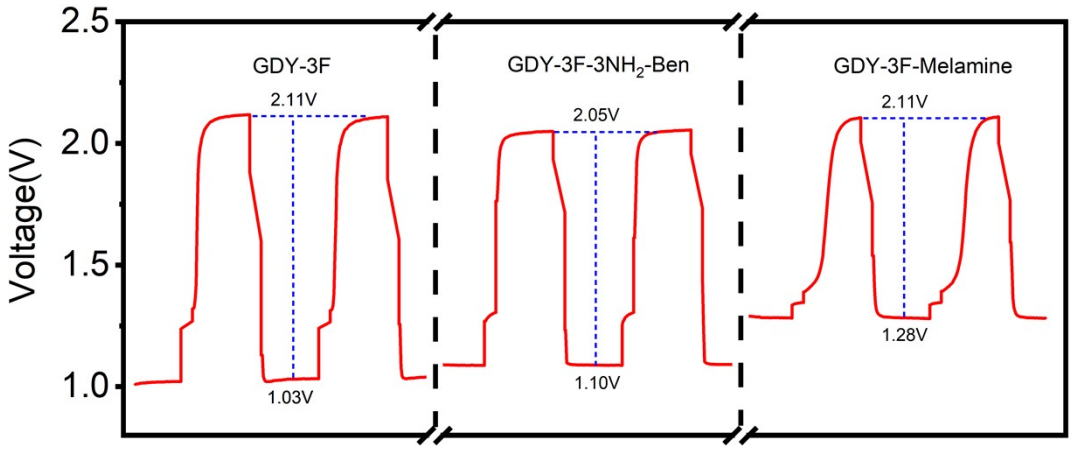

Fig. S12 Comparison of voltage variation in charge-discharge process of zinc-air batteries based on GDY-3F, GDY-3F-3NH_2-Ben and GDY-3F-Melamine systems.

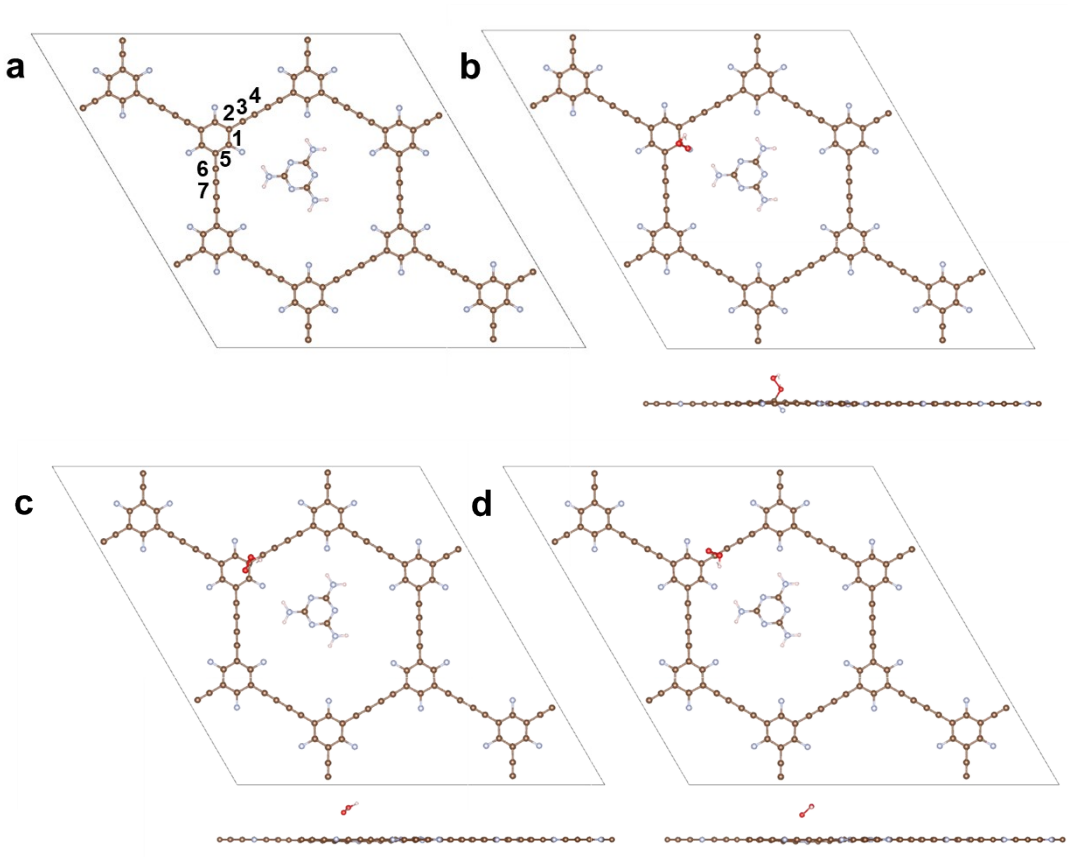

Fig. S13 The atomic configurations of (a) GDY-3F-Melamine substrate with 7 labeled possible active sites, (b)-(d) ORR intermediate *OOH at different site, from C1 to C3, respectively.

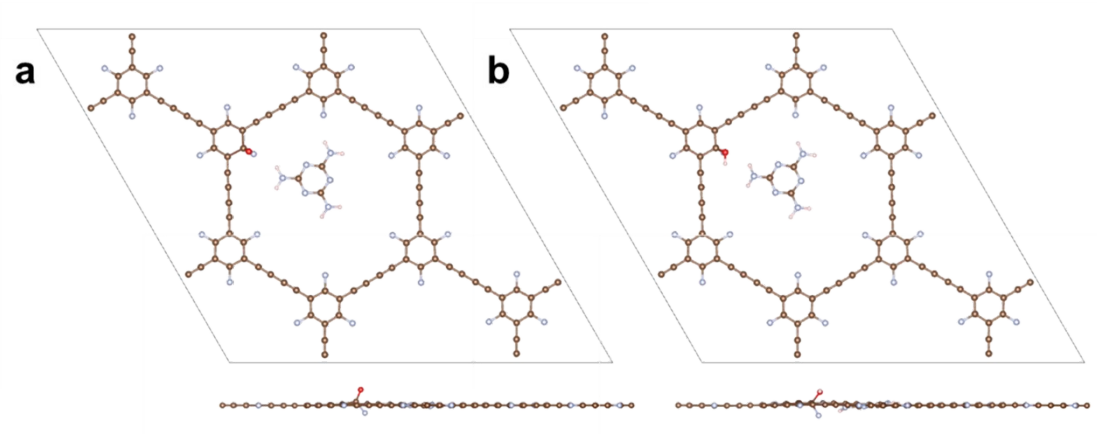

Fig. S14 The atomic configurations of ORR intermediates adsorbed to (a) O and (b) OH of GDY-3F-Melamine at site C1.

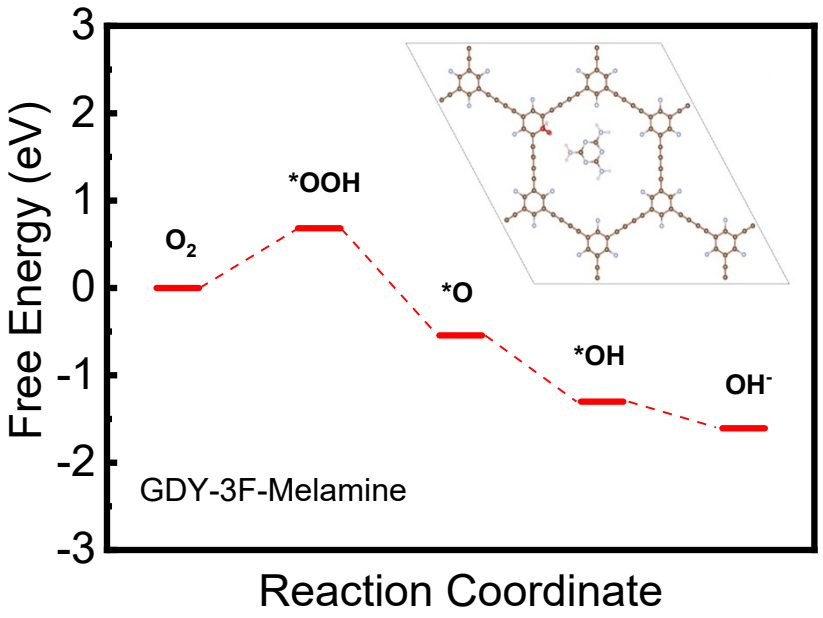

Fig. S15 The free energy diagrams for ORR at site C1 on GDY-3F-Melamine at 0 V (vs. standard hydrogen electrode, SHE) in alkaline solution (pH = 14.0). Inset is the atomic configuration of *OOH at site C1.

Table S1 Comparison of synthesis method and zinc-air battery performance between our work and other related or recent works

Catalyst	Synthesis Method	Peak Power Density (mW cm^{-2})	Specific Capacity (mAh g_{Zn}^{-1})	Energy Density (Wh kg_{Zn}^{-1})	Cycling Stability	Reference
GDY-3F-Melamine	Supra-molecular strategy	94.1	707.8	700.3	>1000 cycles	This work
N, F, B doped carbon fiber	Electrospinning-thermal strategy	-	555	-	>120cycles; >800 min	6
N, P, F doped carbon nanosphere	Pyrolysis strategy	144	-	-	385 cycles	7
N, F, S doped carbon nanofiber	Electrospinning-carbonization strategy	127.5	826.4	991	600 cycles	8
N, F doped porous carbon	Carbonization strategy	157	-	-	200 cycles	9
N, F doped porous carbon	Carbonization strategy	116	-	-	88 h	10
B, N, F doped carbon porous nanofiber	Electrospinning-carbonization strategy	99.4	791.5	-	600 cycles; 200h	11
N, F doped graphdiyne	Pyrolysis strategy	86	~400	-	-	12
N doped graphdiyne	Pyrolysis strategy	84	693	-	450 cycles; 300h	13
Pyridinic N doped graphdiyne	Polymerization strategy	130	647	-	225 cycles; 150h	5
sp-hybridized N doped graphdiyne	Pyrolysis strategy	195.7	-	-	8h	14
$FeNi_3$/ $FeNi_3N$	Hydrothermal Strategy	157	753	881	590 cycles	15

Supplemental Reference

1. P. Yin, T. Yao, Y. Wu, L. Zheng, Y. Lin, W. Liu, H. Ju, J. Zhu, X. Hong, Z. Deng, G. Zhou, S. Wei and Y. Li, Single Cobalt Atoms with Precise N-Coordination as Superior Oxygen Reduction Reaction Catalysts, *Angew. Chem. Int. Edit.*, 2016, **55**, 10800-10805.

2. J. K. Nørskov, J. Rossmeisl, A. Logadottir, L. Lindqvist, J. R. Kitchin, T. Bligaard and H. Jónsson, Origin of the Overpotential for Oxygen Reduction at a Fuel-Cell Cathode, *J. Phys. Chem. B*, 2004, **108**, 17886-17892.

3. J. Rossmeisl, Z. W. Qu, H. Zhu, G. J. Kroes and J. K. Nørskov, Electrolysis of water on oxide surfaces, *J. Electroanal. Chem.*, 2007, **607**, 83-89.

4. F. Calle-Vallejo, J. I. Martínez and J. Rossmeisl, Density functional studies of functionalized graphitic materials with late transition metals for oxygen reduction reactions, *Phys. Chem. Chem. Phys.*, 2011, **13**, 15639-15643.

5. Q. Lv, N. Wang, W. Si, Z. Hou, X. Li, X. Wang, F. Zhao, Z. Yang, Y. Zhang and C. Huang, Pyridinic nitrogen exclusively doped carbon materials as efficient oxygen reduction electrocatalysts for Zn-air batteries, *Appl. Catal. B: Environ.*, 2020, **261**, 118234.

6. H.-F. Wang, C. Tang, B. Wang, B.-Q. Li, X. Cui and Q. Zhang, Defect-rich carbon fiber electrocatalysts with porous graphene skin for flexible solid-state zinc–air batteries, *Energy Storage Mater.*, 2018, **15**, 124-130.

7. Y. Zheng, H. Song, S. Chen, X. Yu, J. Zhu, J. Xu, K. A. I. Zhang, C. Zhang and T. Liu, Metal-Free Multi-Heteroatom-Doped Carbon Bifunctional Electrocatalysts Derived from a Covalent Triazine Polymer, *The Journal of Physical Chemistry BSmall*, 2020, **16**, 2004342.

8. H. Li, T. A. Ha, S. Jiang, C. Pozo-Gonzalo, X. Wang, J. Fang, P. C. Howlett and X. Wang, N, F and S doped carbon nanofibers generated from electrospun polymerized ionic liquids for metal-free bifunctional oxygen electrocatalysis, *Electrochim. Acta*, 2021, **377**, 138089.

9. Y.-N. Sun, J. Yang, X. Ding, W. Ji, A. Jaworski, N. Hedin and B.-H. Han, Synergetic contribution of nitrogen and fluorine species in porous carbons as metal-free

and bifunctional oxygen electrocatalysts for zinc–air batteries, *Appl. Catal. B: Environ.*, 2021, **297**, 120448.

10. Y. Zhao, Y. Liu, Y. Chen, X. Liu, X. Li and S. Gao, A treasure map for nonmetallic catalysts: optimal nitrogen and fluorine distribution of biomass-derived carbon materials for high-performance oxygen reduction catalysts, *J. Mater. Chem. A*, 2021, **9**, 18251-18259.

11. Y. Wang, R. Gan, S. Zhao, W. Ma, X. Zhang, Y. Song, C. Ma and J. Shi, B, N, F tri-doped lignin-derived carbon nanofibers as an efficient metal-free bifunctional electrocatalyst for ORR and OER in rechargeable liquid/solid-state Zn-air batteries, *Appl. Surf. Sci.*, 2022, **598**, 153891.

12. S. Zhang, Y. Cai, H. He, Y. Zhang, R. Liu, H. Cao, M. Wang, J. Liu, G. Zhang, Y. Li, H. Liu and B. Li, Heteroatom doped graphdiyne as efficient metal-free electrocatalyst for oxygen reduction reaction in alkaline medium, *J. Mater. Chem. A*, 2016, **4**, 4738-4744.

13. T. Lu, X. Hu, J. He, R. Li, J. Gao, Q. Lv, Z. Yang, S. Cui and C. Huang, Aqueous/solid state Zn-air batteries based on N doped graphdiyne as efficient metal-free bifunctional catalyst, *Nano Energy*, 2021, **85**, 106024.

14. Y. Zhao, J. Wan, N. Yang, R. Yu and D. Wang, sp-Hybridized nitrogen doped graphdiyne for high-performance Zn–air batteries, *Mater. Chem. Front.*, 2021, **5**, 7987-7992.

15. Y. Niu, S. Gong, X. Liu, C. Xu, M. Xu, S.-G. Sun and Z. Chen, Engineering iron-group bimetallic nanotubes as efficient bifunctional oxygen electrocatalysts for flexible Zn–air batteries, *eScience*, 2022, **2**, 546-556.